



Conductivity Evolution in Propped Fractures During Reservoir Drawdown

Jiayi Yu¹ · Jiehao Wang² · Shugang Wang³ · Yan Li² · Amit Singh² · Peggy Rijken² · Derek Elsworth¹

Received: 22 October 2020 / Accepted: 23 January 2022 / Published online: 28 February 2022
© The Author(s), under exclusive licence to Springer-Verlag GmbH Austria, part of Springer Nature 2022

Abstract

We investigate the evolution of fracture conductivity as a function of proppant loading concentration under varying effective stresses as an analog to reservoir drawdown. In particular, we define the relative impacts and interactions between proppant crushing, proppant embedment, compaction and particle rearrangement and their impacts on fluid transport. Proppant of realistic concentrations is sandwiched between split core-plugs of Marcellus shale that accommodates embedment as well as rigid steel that excludes it. Impacts of proppant crushing and embedment and roles of particulate transport in fracturing-fluid clean-up are defined. Experiments are performed under triaxial stresses with independent control on confining stress and pore pressure. Normal loading is incremented to represent reservoir drawdown with conductivity evolution recorded continuously via flow-through of brine (20,000 mg/L KCl). Proppant embedment is characterized pre- and post-test by white light optical profilometry with pre- and post-test particle size distributions of the proppant defining the impact of proppant crushing. The conductivity of propped fractures decreases by up to 95% as effective stress is increased by 50 MPa (7000 psi). This reduction is broadly independent of whether the fracture walls are rigid or deformable. The stress-sensitivity of conductivity is generally muted with increasing proppant loading concentration. We normalize fracture conductivities to equivalent permeabilities of the proppant pack to directly compare pack permeabilities. Low proppant concentrations return higher permeability at low effective stresses but lower permeability at high effective stress, relative to high proppant concentrations. This results since proppant crushing and embedment are both mitigated with increasing proppant loading concentration, as more displacement degree of freedom are added to the system and provide accommodation for interior compaction and rearrangement. Extended effective stress holding times (24 h vs < 1 h) and proppant “aging” exert little impact on transient changes in fracture conductivity.

Highlights

- Propped shale fracture conductivity decreases as the effective pressure increases. Stress sensitivity reduces with increasing effective stress.
- Reduced proppant loading concentration results in greater proppant embedment, increased proppant crushing and greater circularity.
- The mechanisms for permeability reduction between different proppant loading concentrations (thicknesses) are different.
- Where proppants are injected at low loading concentrations, the most effective approach to maintain permeability is to reduce proppant embedment.
- Where high proppant loading concentrations are attained, the major impairment mechanism is proppant compaction and rearrangement.

✉ Jiayi Yu
jzy200@psu.edu

¹ Department of Energy and Mineral Engineering, EMS Energy Institute and G3 Center, Pennsylvania State University, University Park, PA 16802, USA

² Chevron, ETC, 1500 Louisiana St, Houston, TX 77002, USA

³ Consultant, Houston, USA

Keywords Proppant · Propped fracture conductivity · Proppant embedment · Proppant crushing

1 Introduction

Conventionally, hydrocarbons have been recovered from sandstone or carbonate reservoirs where they are trapped in well-connected systems of pores and fractures. With recent advancements in recovery techniques, such as horizontal drilling and hydraulic fracturing, oil and gas can also be recovered unconventionally from less-permeable reservoirs such as tight sands, coal beds or shale formations. During hydraulic fracturing, fluid is injected at high flowrate with the resulting pressure buildup inside the borehole driving hydraulic fractures and reactivating favorably oriented pre-existing fractures. Proppants are then pumped in to hold fractures open, retaining a high-conductivity flow path for oil and gas production (Arthur et al. 2009; Vengosh et al. 2014). Employing these techniques has driven vigorous development in the energy sector over the last 2 decades and delivered energy security to the United States. Such reservoir stimulation techniques require that propped fractures be large, return large increases in permeability and remain conductive over extended reservoir lifetimes as in situ stresses and deformations evolve (Mayrhofer et al. 2006).

However, the conductivity of propped fractures may decrease dramatically with time, even for dormant wells (Cikes 1996). The relative reduction can be up to ~95% (Palisch et al. 2007). Individually extensive but largely separate literatures have addressed the principal mechanisms controlling the evolution of propped fracture conductivity. These include the role of intrinsic mechanical characteristics of both rock and proppant, proppant embedment, proppant crushing, proppant compaction and particle rearrangement, proppant pack concentration (thickness), long term rock creep and poroelastic interactions (Yasuhara et al. 2003; Weaver et al. 2007; Pope et al. 2009; Terracina et al. 2010; Lee et al. 2010; Zhang et al. 2013; Briggs et al. 2014; Wang and Elsworth 2018).

The constituent mineral contents of shale influence fracture conductivity (Briggs et al. 2014) with the presence of clay minerals presenting the greatest impact—typically in creep closure. Clay-rich shales exhibit significant conductivity reduction under high closure pressures (Zhang et al. 2015) as impacted by the altering of rock strength and susceptibility to proppant embedment (Alramahi et al. 2012). A variety of different materials have been used as proppants—both naturally occurring minerals and manufactured composites. By far, natural sand proppant is the most widely used and also the least expensive. Conversely, sand proppant is less resistant to crushing than manufactured composites,

especially under high closure stresses, resulting in a potential loss of function (Beckwith 2011; Liang et al. 2016).

Particle crushing and spalling from fracture walls liberate fines that may migrate and plug pore throats. The potential for plugging by proppant fines is largely determined by proppant grain shape, grain breakage pattern and stress–strain response of the proppant pack and is indexed by the change in particle-size distribution (Kurz et al. 2013; Zhang et al. 2015). An evolving broader particle size distribution and range of particle shapes result in tighter packing and denser compaction. However, the relative contribution of these factors will vary, dependent on specific circumstances. Sand characterization and crushing tests on Jordan Formation frac sand show a permeability reduction of more than 40% at a stress of 20 MPa, driven by particle rearrangement and compaction that is supplanted by a further 30% decrease at 40 MPa driven by particle breakage and size reduction (Zheng and Tannant 2016).

Propped fracture conductivity and permeability typically increase as proppant loading concentration increases. The increase in conductivity is due to the increase in flow cross section as nominal permeability remains near-constant. However, permeability may also increase as multilayer arrangements of proppant provide more contact points to resist stress and mitigate proppant crushing and embedment and thereby minimize loss of permeability (Wen et al. 2007; Zhang et al. 2013; Briggs et al. 2014; Elsarawy and Nasr-El-Din 2018). Conversely, the increased number of contact points may also result in denser compaction, accompanied by grain rearranging into closer packing configuration and reduction in pore throat diameter and porosity, potentially decreasing conductivity.

Additional reduction in conductivity may also evolve over the long term—resulting from both enhanced rock creep (Zhang et al. 2015) and proppant-pack diagenesis (Lee et al. 2010; Mittal et al. 2018), in which mechanical stresses and chemical compaction contribute to the changes in conductivity via changes in porosity. Reported reductions range from of the order of ~19–25% under recreated in situ stresses and at room temperature (Zhang et al. 2015) and over a holding period of 52 h, to of the order of ~75% under higher temperature and over periods of more than 1000 days (Lee et al. 2010)—driven by pressure solution and other thermally activated and fluid mediated mechanisms.

A variety of studies have explored the impact of coupling mechanisms on the evolution of conductivity in propped fractures under varied effective stress states. These studies offer conflicting views of whether conductivity either

increases or decreases as a function of proppant loading under incremented effective stress. We address this uncertainty by exploring mechanistic controls on conductivity evolution through observations from highly constrained experiments.

We measure the evolution of conductivity and other index characteristics of propped fractures with changing stress for different proppant loading concentrations (thicknesses) as an analog to reservoir drawdown. We compare conductivity evolution between parallel experiments either allowing (shale fractures wall) or excluding (steel platens) proppant embedment and over the short and long term (24 h). We address the following questions: (1) what are the dominant conductivity impairment mechanisms for different proppant loading concentrations and under incremented effective stress? (2) What are the interplays between the impairment mechanisms? (3) What strategies are available to mitigate conductivity loss?

2 Experimental Methods

We complete flow-through experiments on split cores containing a proppant pack under recreated in situ stresses. Different proppant pack loading concentrations (thicknesses) establish systematic control on conductivity evolution during pressure drawdown.

2.1 Sample Preparation

The Marcellus shale formation extends in the subsurface from New York State in the north to northeastern Kentucky and Tennessee in the south and is the most prolific natural gas-producing formation in the Appalachian basin (U.S. Energy Information Administration. “Marcellus Shale Play Geology Review”. 2017). We use Marcellus samples that contain (XRD) 60.2% quartz, 20.5% muscovite, 13.5% nacrite, 4.3% pyrite and 1.5% clinocllore.

A block sample is cored parallel to bedding into cylinders 50 mm (2 inches) in length and 25 mm (1 inch) in diameter. The cylinders are longitudinally split-in-half (Fig. 1b) and the fracture

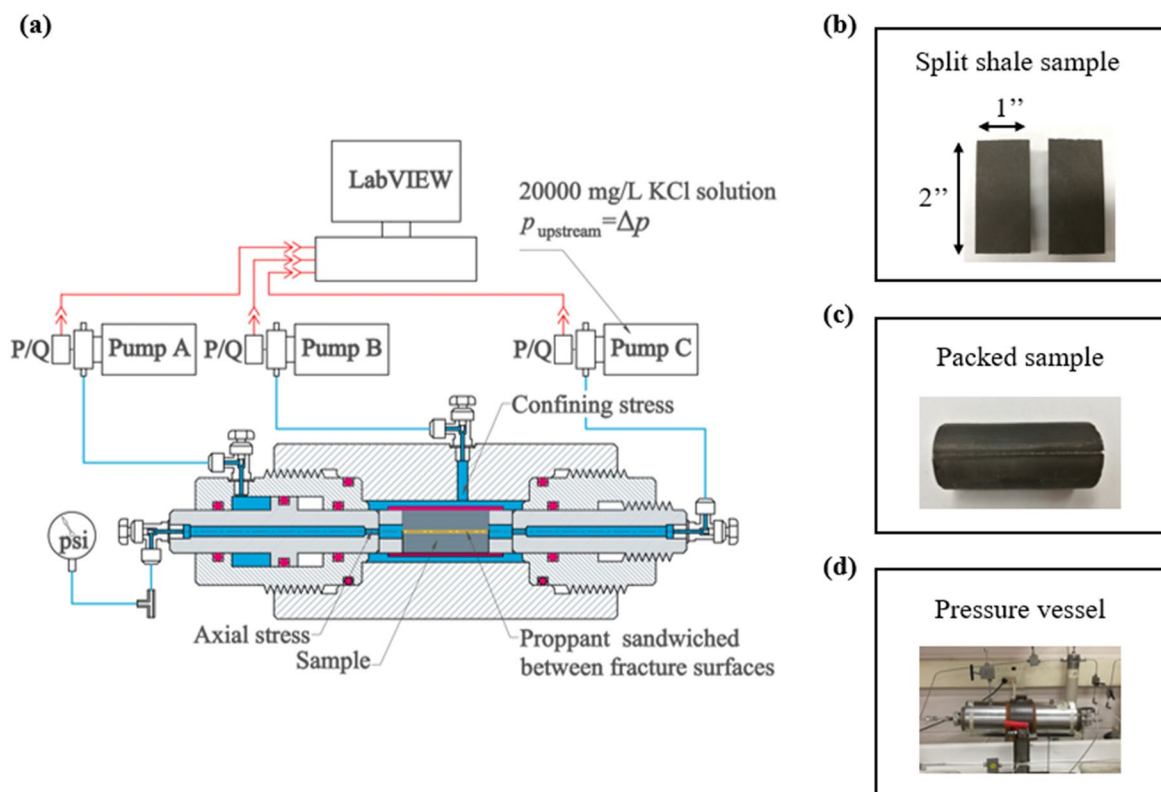


Fig. 1 a Schematic of experimental arrangement for the measurement of proppant conductivity. ISCO pumps A and B supply controlled axial and confining pressures; pump C supplies sample through-flow with upstream pressure prescribed and resulting fluid flow rate

monitored; downstream pressure is atmospheric. b Split half-cylindrical shale sample. c Cylindrical sample containing fracture surface embedded with proppant. d Triaxial pressure vessel (Temco)

surfaces are polished using #360 grit sandpaper to provide consistent pre-test fracture surface roughness for all experiments. The initial conditions of the shale fractures—specifically surface roughness—are characterized by White Light Optical Profilometry, to confirm the repeatability of this aspect of the experiments.

2.2 Permeating Fluids and Proppants

Brine (20,000 mg/L KCl solution) is used as the permeant, representing a typical flowback water that returns to the surface following completion of the hydraulic fracturing process. The proppant used for this study is 100-mesh sand—a standard material—with a cumulative particle size distribution (PSD) in terms of cumulative percentage by both number (left y-axis) and by volume (right y-axis) of particles as shown in Fig. 2. The corresponding mesh numbers to the particle sizes are also provided in Fig. 2. The 100-mesh sand mostly consists of sands between 50 and 140 mesh. Proppants are well mixed before each experiment to limit particle segregation.

As shown in Fig. 2, the cumulative percentages of the same PSD by volume and by number seem surprisingly disparate; however, they are indeed congruent and consistent. Dependent on the equivalent diameter, the pre-test proppant particles are divided into three distinct families. These families represent large, intermediate and small particles of $> 200 \mu\text{m}$, ~ 50 to $100 \mu\text{m}$, and $< 10 \mu\text{m}$, respectively. Assuming 100 spherical proppant particles, then an average PSD dictates that ~ 25 will be small particles ($< 10 \mu\text{m}$), ~ 5 intermediate particles (~ 50 to $100 \mu\text{m}$) and ~ 10 are large particles ($> 200 \mu\text{m}$). According to the cumulative percentage by number, the total volume of each size fraction is calculated as

$$V_{\text{total}} = \frac{4}{3} \pi r^3 \times n, \quad (1)$$

in which r is the mean particle radius and n is the number of particles.

The calculation indicates that the total volume of large particles ($> 200 \mu\text{m}$) is ~ 50 times that of that of intermediate particles (~ 50 to $100 \mu\text{m}$), and > 1000 times of that of the small particles ($< 10 \mu\text{m}$). This suggests that even though there are a large number of small particles, the total volume of this size fraction is negligible compared to even the much smaller number of larger particles. The volume percentage is representative of the overall quantity. Thus, measurements of cumulative percentage by number, indeed, agree with the observations of cumulative percentage by volume (Fig. 2).

2.3 Experimental Setup

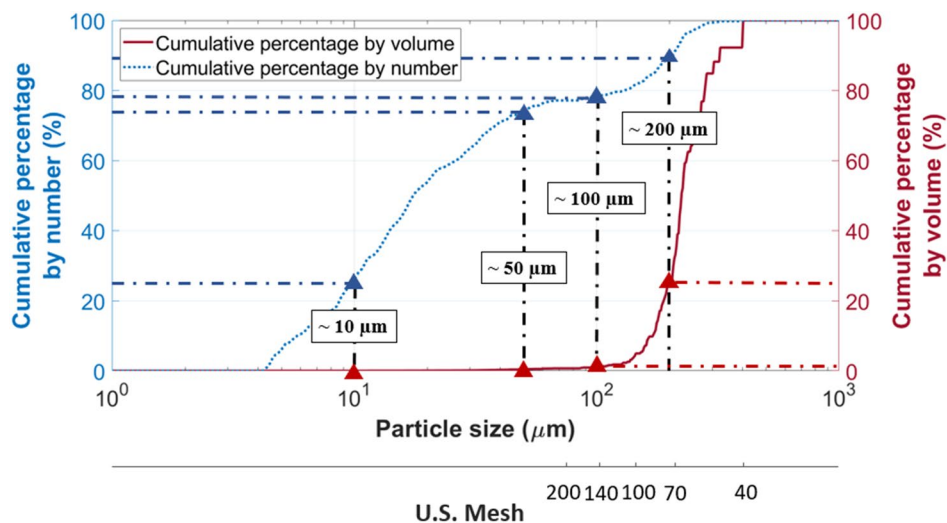
The experiments are performed in a triaxial testing apparatus with independent control on normal stress, pore pressure and axial stress. The schematic configuration of the experimental setup is shown in Fig. 1(a).

2.4 Experimental Procedure and Conditions

Conductivity measurements are completed through the following steps:

- (1) Proppant is placed uniformly between the split halves of the shale core (Fig. 1c).
- (2) The packed sample is loaded into the triaxial pressure vessel (Fig. 1d).
- (3) Axial and normal (confining stress in this configuration) stresses are synchronously incremented and with uniform magnitude to the desired value.
- (4) Conductivities are measured by injection of brine (20,000 mg/L KCl solution) at that constant stress.

Fig. 2 Pre-test PSDs in terms of cumulative percentage by number (left y-axis) and by volume (right y-axis)



- (5) Stresses are incremented to a new magnitude (#3) and conductivity measured (#4).

Fluid is injected into the upstream end of the sample at constant pressure and discharges from the downstream end at atmospheric pressure. The effective stress is defined as the difference between the confining normal stress and pore pressure (Biot coefficient of unity). The pore pressure drop across the fracture is limited to ~30 kPa (~0.4% of the minimal normal stress) enabling the effective stress along the fracture to be considered effectively constant. Fluid flow rates are sufficiently slow to prevent excessive washout of the proppant. Short-term (~20–25 min) and long-term (24 h) conductivity measurements examine the impact of “aging”. Experiments are performed at room temperature (20 °C) with both proppants and shale samples are retained dry before the experiments.

2.5 Pre- and Post-experiment Analysis

Fracture surface roughness of the shale samples are characterized before then after the experiments by White Light Optical Profilometry (Zygo NewView 7300 profilometer, 20× objective lens and data processing by Mx software (Fig. 3a)). Fifteen randomly-located observation patches (0.836 mm×0.836 mm in dimension) are captured from the surface of each specimen. To examine proppant crushing, proppant particles are scanned both before then after experiments using high resolution microscopy [Malvern Morphologi G3SE (Fig. 3b)] to define particle size distribution and particle morphology.

2.6 Evaluation of Conductivity and Permeability

Conductivity (*C*) reflects the fluid transmission capability of the entire proppant-filled fracture and is calculated from Darcy’s law as

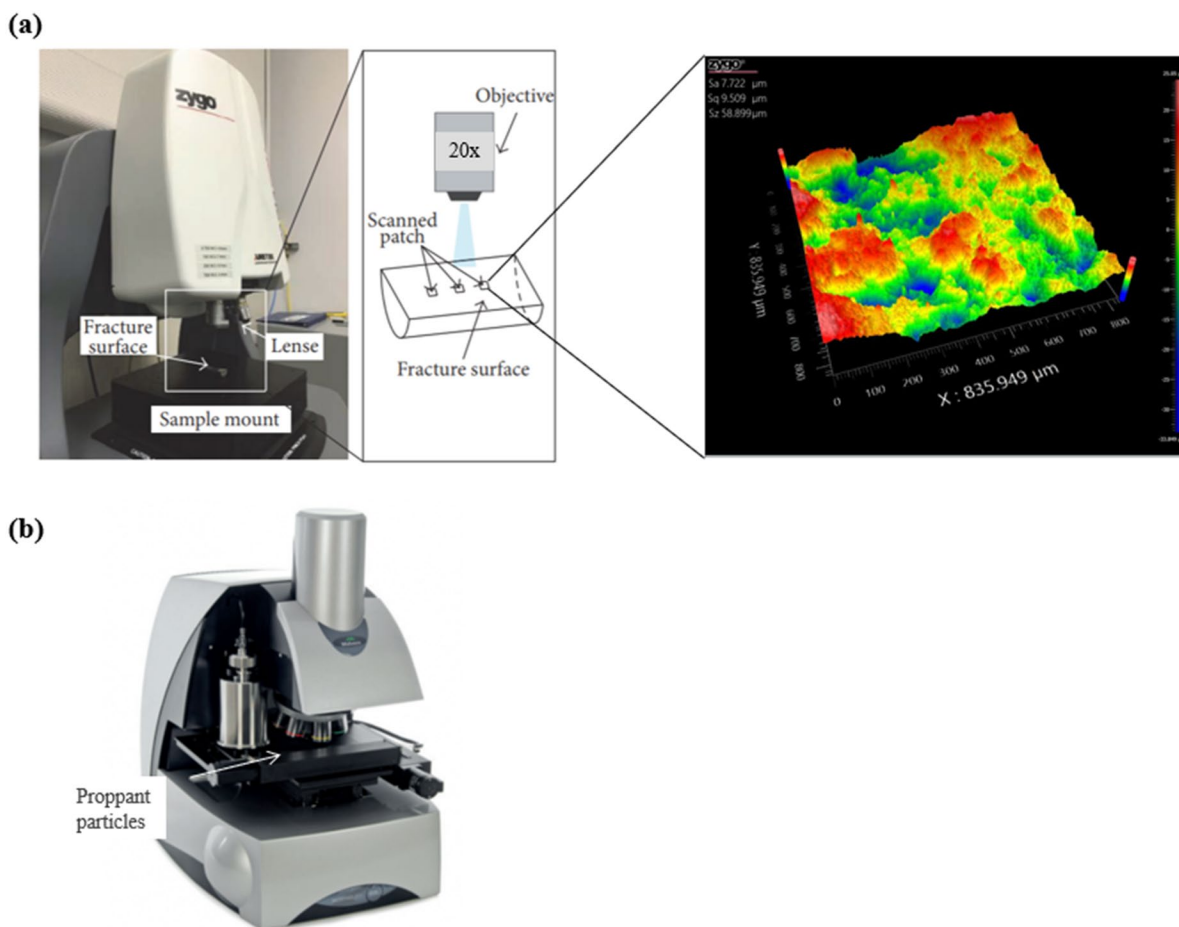


Fig. 3 **a** 3D white-light optical surface profiler for characterizing statistical roughness of the fracture surface (modified from Fang et al. 2017). **b** High-resolution microscope-based automated imaging sys-

tem for determining particle size distribution and particle morphology (modified from “Size Ranges for Malvern Instruments”)

$$C = \frac{\mu L Q}{w \Delta p}, \quad (2)$$

where μ is fluid viscosity (8.9×10^{-4} Pas), L is flow path length (0.0508 m), w is flow path width (0.0254 m), Q is flow rate (m^3/s) and Δp (Pa) is the pressure difference between the upstream and downstream along the fracture.

The capacity of the proppant pack to transport fluid is characterized by an equivalent propped fracture permeability (K), defined as the conductivity (C) normalized by the initial fracture aperture (h). Initial fracture aperture is not measured and is difficult to characterize, but may be approximated as the ratio of proppant bulk density (kg/m^3) to proppant loading concentration (kg/m^2), as

$$K [L^2] = \frac{C [L^3]}{h [L]} = C [L^3] \times \frac{\rho_{\text{bulk}} [M \times L^{-3}]}{c_{\text{proppant}} [M \times L^{-2}]}, \quad (3)$$

where ρ_{bulk} is $1630 \text{ kg}/\text{m}^3$.

Such an equivalent permeability enables direct comparison between experiments with different proppant loading concentrations, highlighting the loss of function of the proppant itself, as a result of crushing or embedment. However, this parameter assumes that fracture aperture remains constant throughout each experiment even though it will decrease with effective stress increments—representing a minor artifact in its interpretation. However, previous study on fracture aperture evolution vs. effective stress shows a nearly proportional fracture aperture to proppant loading concentrations, and a linear set of change in fracture aperture as a function of increasing effective stress (Fig. 4) (modified from Zhang et al. 2017). Therefore, this artifact may impact the value of permeability for each parallel experiment but will not change the overall trend in response.

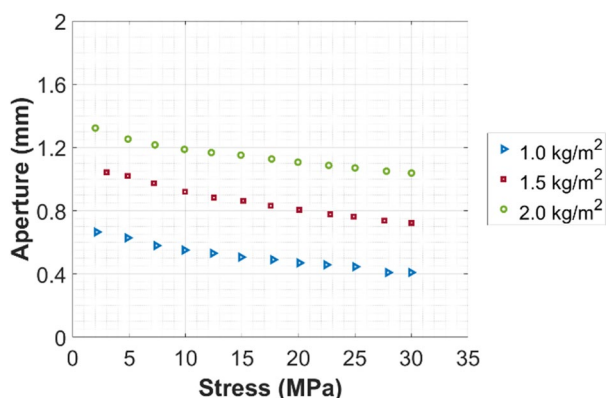


Fig. 4 Experimental results of fracture aperture vs. effective stress for three different proppant loading concentrations with 40/70-mesh proppant (modified from Fig. 4 in Zhang et al. 2017)

3 Experimental Results

We present key observations both pre- and post-experiment to compare conductivity and permeability evolution between suites of experiments either allowing (shale fractures wall) or excluding (steel platens) proppant embedment and over both the short- and long-term. Relative contributions and interactions of proppant crushing and embedment and proppant compaction in impacting conductivity are defined. Experimental variables are effective stress, proppant loading concentration and the embedment characteristics (rigid or deformable) of the fracture walls.

3.1 Role of Effective Stress

An initial effective stress of 1000 psi (6.9 MPa) was first applied to the samples and successively incremented by 2000 psi (~10 MPa) to 8000 psi (55.2 MPa) as a maximum stress. The fractures were propped by 100-mesh sand at proppant loading concentrations of 0.1, 0.25, 0.5 and 1 lb/ft^2 (0.49, 1.22, 2.44 and 4.88 kg/m^2) in successive experiments. A single layer of this close-packed proppant weighs ~0.33 g; thus, the proppant loading concentrations used here are approximately equivalent to 2 to 20 layers.

Figure 5a, b shows the evolution of conductivity when sandwiched between both Marcellus shale and steel, respectively. Conductivity decreases by up to 95% as the effective stress increases by 7000 psi (48.3 MPa), broadly independent of whether the fracture walls are deformable or rigid. The normalized conductivities in Fig. 5c, d are normalized relative to the conductivity at the initial effective stress, for each of the four proppant concentrations. This demonstrates that the greatest stress sensitivity is at low effective stress which gradually mutes as effective stress is increased.

3.2 Role of Proppant Loading Concentration

For Marcellus shale, as shown in Fig. 6a, a lower proppant concentration results in a higher initial equivalent permeability at low effective stress (6.9 MPa), while a higher proppant concentration maintains a slightly higher permeability under high effective stress (55.2 MPa). The permeability reduction is most extreme for the lowest (0.49 kg/m^2) proppant concentration. In all cases, the permeability reduction over each stress increment reduces as the confining stress increases and this sensitivity to stress decreases as the proppant loading concentration increases. For steel, as shown in Fig. 6b, the trend is broadly similar, except that a higher proppant loading concentration always results in a lower permeability than for a lower proppant concentration, over all effective stresses. It is notable that under the maximum effective

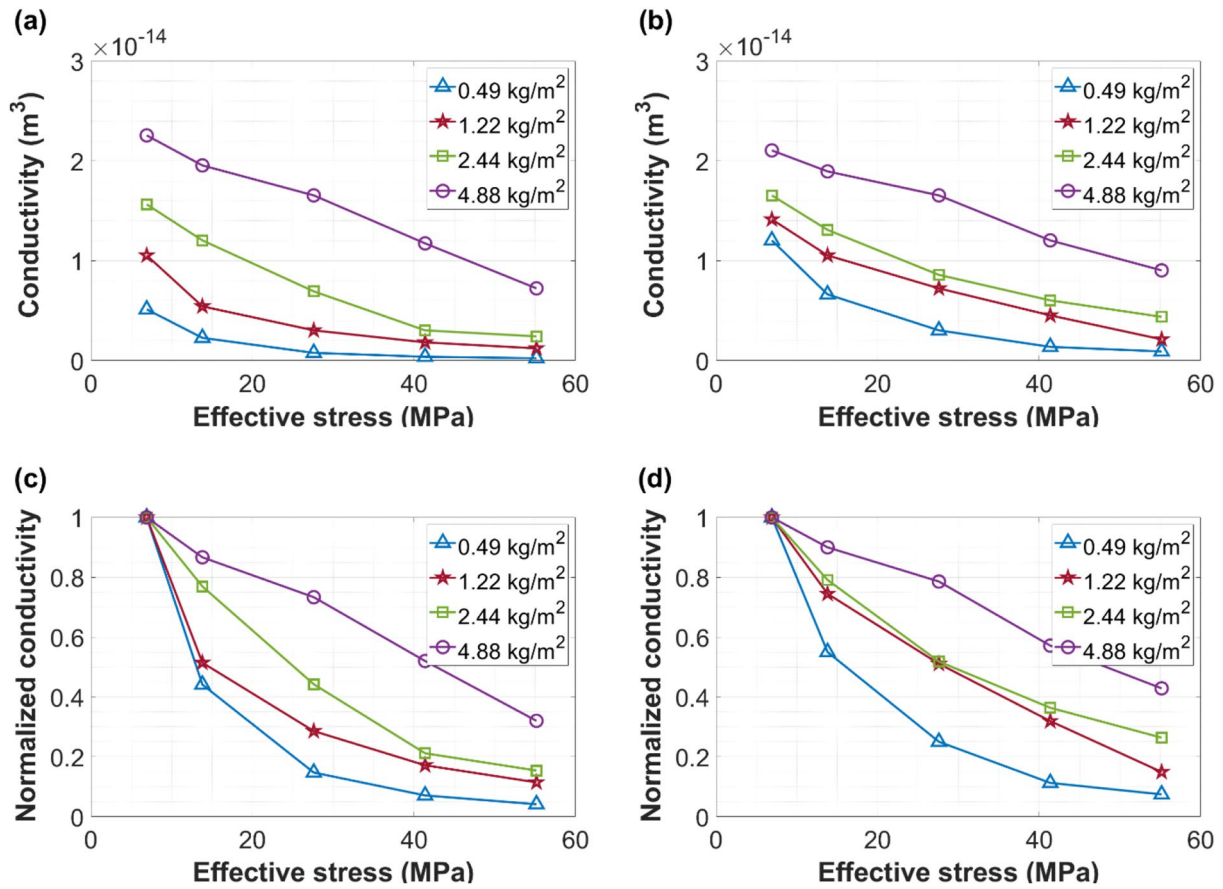


Fig. 5 Evolution of fracture conductivity with effective stress for **a** Marcellus shale (embedment) and with **b** steel platens (no embedment). Normalized conductivity (proppant pack permeability) for **c** Marcellus shale and with **d** steel platens

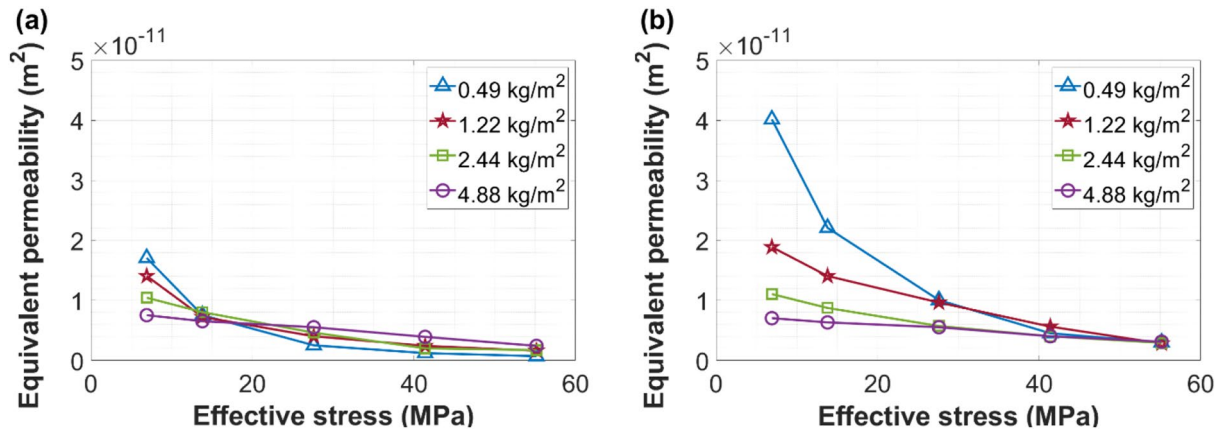


Fig. 6 Evolution of fracture permeability both **a** with embedment (Marcellus shale) and **b** where embedment is excluded (steel platens)

stress of 55.2 MPa, all proppant concentrations asymptote to a minimum permeability—presumably representing a maximum limit in compaction.

This distinction demonstrates the effect of embedment on fracture conductivity, the mechanism of which will be discussed more in detail in Sect. 3.3.

At a given effective stress, permeability should be constant between all proppant loading concentrations, since

Fig. 7 Illustration of multilayered samples suggesting high flow-rate channels developing at the interface between the proppant pack and the fracture

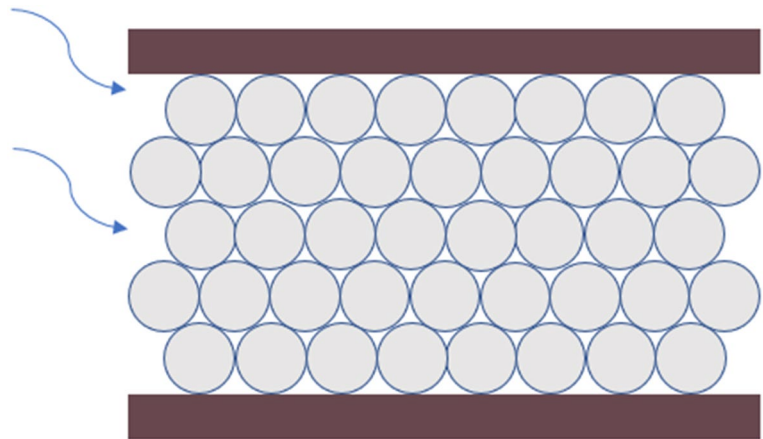


Table 1 Surface roughness parameters both pre- and post-test for the fracture surface

Sample #	$S_a(\mu\text{m})$	$S_q(\mu\text{m})$	$S_z(\mu\text{m})$
Ground pre-test	0.43	0.56	6.26
0.49 kg/m ² post-test	8.26	10.54	71.83
2.44 kg/m ² post-test	6.93	8.71	57.59
4.88 kg/m ² post-test	4.93	6.37	48.33

permeability is an intrinsic measurement of the state of the proppant pack. However, in our experiments, permeability increases with a decrease in proppant loading concentration. This is consistent with high flow-rate channels developing at the interface between the proppant pack and the fracture—where the packing in contact with the fracture wall is essentially face-centered-cubic rather than body-centered-cubic as in the core of the pack (Fig. 7). This would yield an elevated permeability for low proppant loading concentrations (thin pack) that would decrease as the pack thickened.

3.3 Role of Embedment

Contrasting experiments with Marcellus shale and rigid steel explore the effect of proppant embedment into the fracture walls on conductivity and permeability. Table 1 compares the topographies of post-test shale fracture surfaces for different proppant loading concentrations relative to the ground pre-test surface. Surface roughness parameters include S_a , the arithmetic mean height of asperities, S_z , the maximum height between peak and valley, and S_q , the root mean square height:

$$S_a = \frac{1}{n} \sum_{i=1}^n |y_i|, \tag{4}$$

$$S_z = \frac{1}{l} \sum_{i=1}^s (S_p - S_v)_i, \tag{5}$$

$$S_q = \sqrt{\frac{1}{n} \times \sum_{i=1}^n y_i^2}, \tag{6}$$

where the roughness profile (Fig. 8) contains a total of n equally spaced elevations along a section from the 1st to the i th sampled elevation along the trace; y_i is the vertical distance from the mean line to the i th data point; S_p is the maximum peak height; S_v is the maximum valley depth; and l is the sampling length.

Shale fracture swelling effects are reversible whereas embedment due to plastic deformation of the organic or clay components is destructive and likely irreversible (Meyers 1982). Fractures supported by proppant at the lowest concentration (0.49 kg/m²) return the highest roughness relative to the pre-test (smooth) roughness, by returning the most significant embedment.

In this study, we use S_q as a proxy of the maximum depth of embedment for the purpose of quantifying the effect. The embedment depth for moderate to high loading concentration (2.44kg/m²) is ~80% of that of the lowest concentration (0.49 kg/m²) while that for the highest loading (4.88 kg/m²) is only 60% (Table 1 and Fig. 9). This indicates that embedment depth decreases with higher proppant loading concentration.

An explanation for this observation is that, compared with the extreme condition for a single proppant layer, where particles are sandwiched and point-contact fixed between the two abutting fracture surfaces, a multi-layer proppant distribution possesses many more displacement degrees of freedom. These added degrees of freedom allow the proppant pack to readjust and compact and thereby redistribute particle-to-particle loading within the interior

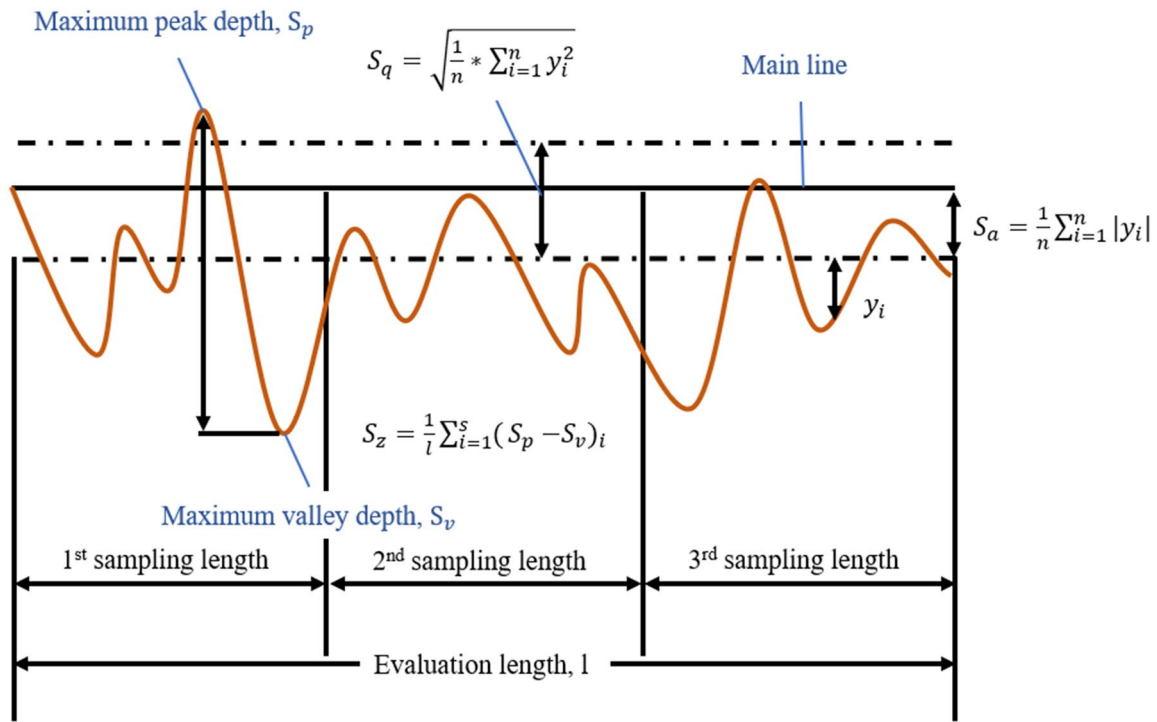


Fig. 8 Surface roughness profile

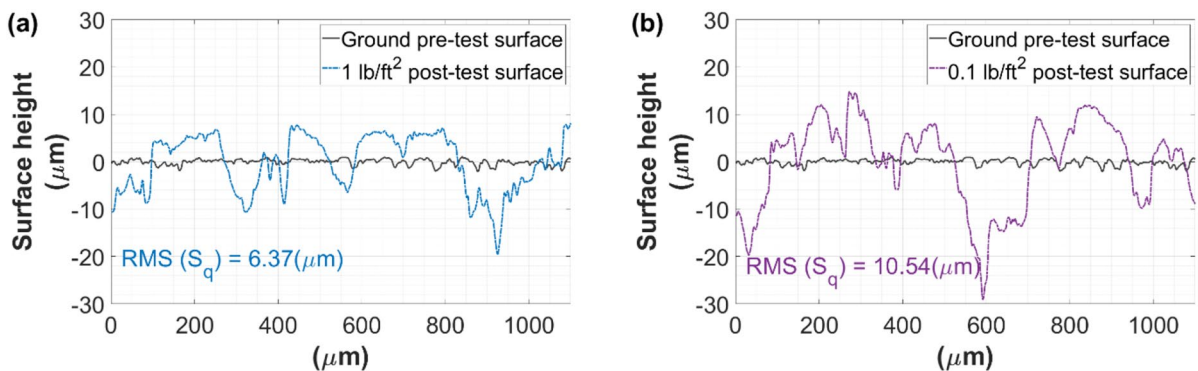


Fig. 9 Comparison of surface height and RMS amplitude S_q between the pristine polished/ground pre-test surface and the post-test fracture surface for proppant loadings of **a** 4.88 kg/m², and **b** 0.49 kg/m²

for a more homogenous stress distribution—limiting particle-to-particle contact stresses.

The ratio of conductivity for the steel fracture relative to that for Marcellus shale at each effective stress magnitude is shown in Fig. 10. For a given proppant loading concentration, embedment reduces fracture conductivity progressively more as effective stress increases. Moreover, when proppant loading concentration is the highest (4.88 kg/m²) the fracture conductivities of both the Marcellus shale and steel remain similar over the full stress

range—indicating, as expected, the reduced sensitivity to stress as the proppant loading concentrations is large.

3.4 Evolution of PSD

The particle size distribution and circularity of proppants evolve during the experiments in response to proppant loading concentrations and the hardness of the fracture surfaces (Fig. 11). For the shale fracture, the post-test proppant may entrain some shale fragments spalled from fracture walls.

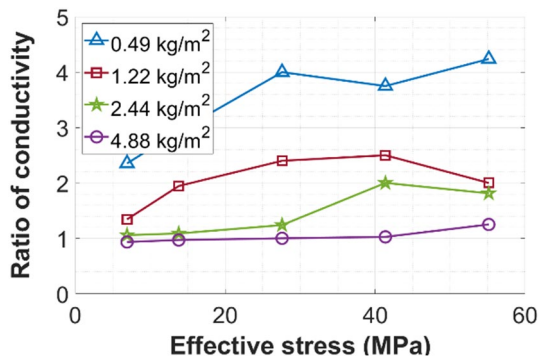


Fig. 10 Ratio of conductivities as a function of effective stress. Conductivity ratio defined as the ratio of the conductivity of a steel fracture to that of Marcellus shale

Apparent from Fig. 11a, b, the particle size distributions show impacts of proppant crushing in all experiments, regardless of proppant loading concentration or fracture wall characteristics. Furthermore, the lowest proppant loading concentration (0.49 kg/m²) exhibits the most profound crushing of proppant, with that degree of crushing decreasing as proppant loading concentration is increased.

Mechanistically, proppant loading concentration impacts the potential for the proppant to compact and redistribute within the fracture—as a result of the increase in displacement degree of freedom as the pack thickens—especially when increased from a monolayer. For a single-layer of proppant, individual particles are directly gripped by two fracture surfaces—the resulting point loading of grains will promote crushing. Conversely, a multilayer distribution provides more contact points to distribute stress and will reduce crushing.

Figure 11c, d shows the evolution of particle circularity of both pre- and post-test, for both shale and steel fracture walls. Together with the evolution of the particle size distribution, this suggests that lower proppant loading concentrations promote crushing and that an increase in circularity results from this elevated crushing – a counter intuitive result. Figure 12 presents the morphology of the proppant, post-test, indicating three distinct families, dependent on equivalent diameter and shape. These families represent large (Fig. 12a), intermediate (b) and small (c) particles of ~ 200 μm, ~ 50 to 100 μm, and < 10 μm, respectively. The “large particles” are of the same order as the largest pre-test particles and thus are considered intact—these

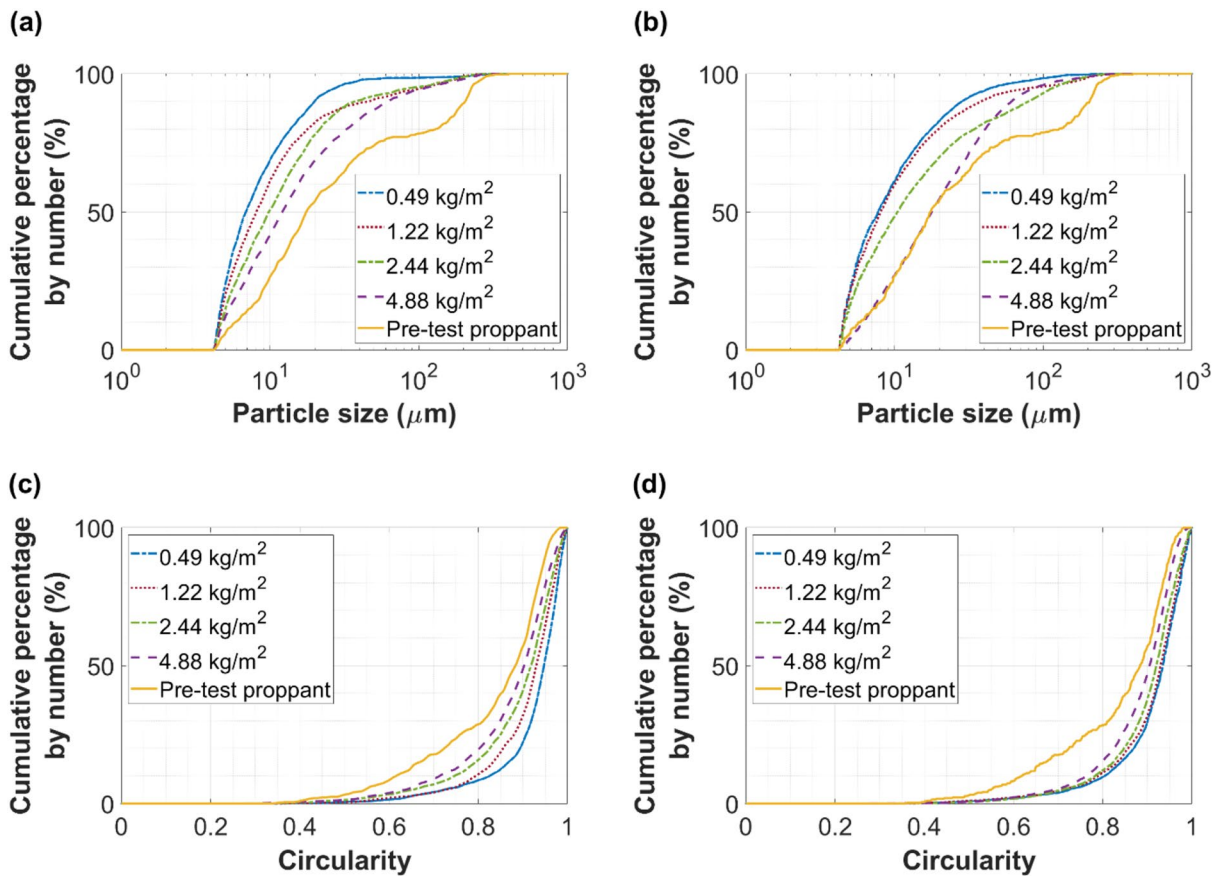


Fig. 11 Particle size distribution and circularity of proppants both before and then after experiments for shale: (a, c), and steel: (b, d) samples

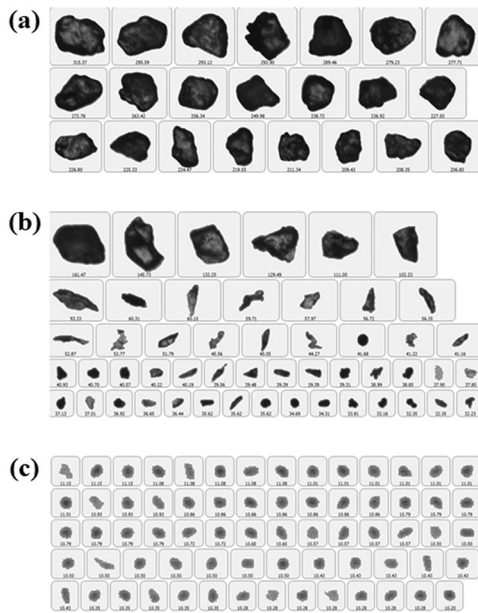


Fig. 12 Imaging of post-test proppants for the lowest (0.49 kg/m²) loading concentration obtained from optical microscopy and grouped as families of: **a** “large”, **b** “intermediate”, and **c** “small” particles of ~200 µm, ~50 to 100 µm, and < 10 µm, respectively

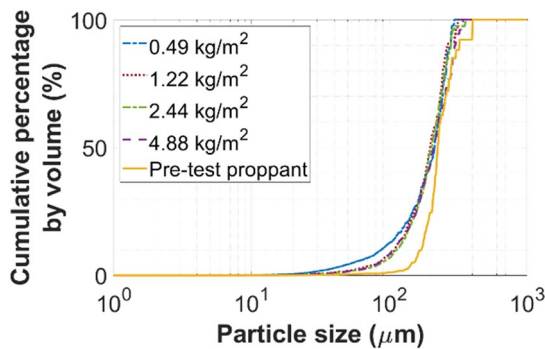
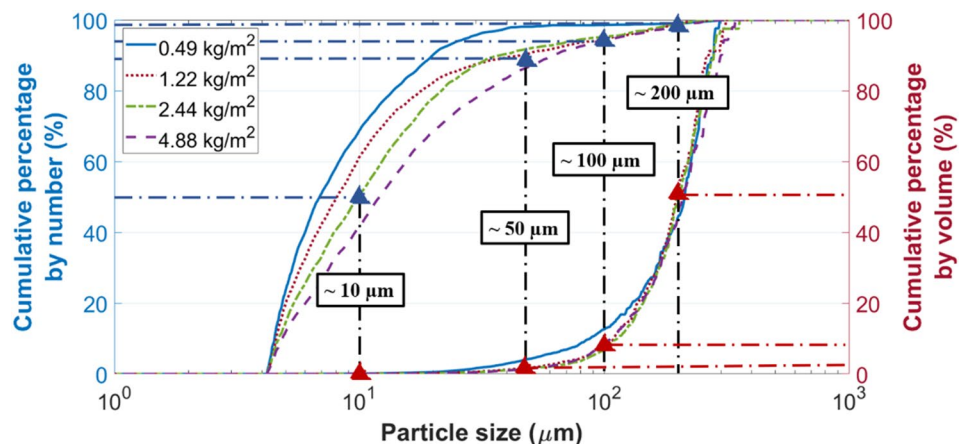


Fig. 13 Pre- and post-test particle size distribution in terms of cumulative percentage by volume

Fig. 14 Post-test PSDs in terms of cumulative percentage by number (left y-axis) and by volume (right y-axis)



remain circular/spherical in form and may be considered as un-crushed. At the opposite end of the distribution, the “small particles” are even more round than the “large particles” with the “intermediate particles” presenting broadly irregular shapes that appear incompletely crushed. From the post-experiment PSD (Fig. 11a, b), the “large particles” comprises < 1%, the “intermediate particles” ~ 10%, with the “small particles” providing the majority number percent at > 80%. We speculate that the large particles first break along crystallographic axes into irregular prismatic intermediate-sized particles that are structurally unstable, due to their aspect ratio, and that these tend to break into equiaxed smaller particles. The population distribution is a direct result of a small number of large particles (~ 1%) producing a larger number of intermediate spalling products (> 10%) that then create a very large number of small equiaxed particles (> 80%) merely as a function of the transition from a long slender prismatic parent.

Figure 13 shows the contrasting particle size distribution in terms of cumulative percentage by volume. This indicates that even though the small particles (< 10 µm) predominate the distribution (> 80%) by number percentage, they represent only a small fraction of the total particle mass or volume (< 1%). The large particles (~ 200 µm) predominate in the mass distribution (> 50%). It is notable that the resulting post-test proppant PSDs are similar between all loading concentrations (Fig. 13)—suggesting that the mode and severity of crushing is independent of proppant concentration. Overall, this reflects the reduced sensitivity of mass percentages relative to number percentages in highlighting changes in the PSDs.

Figure 14 shows post-test PSDs in terms of cumulative percentage by both number (left y-axis) and by volume (right y-axis). Assuming 100 spherical proppant particles, then an average PSD for a proppant concentration of 1.22 kg/m² dictates that ~ 50 will be small particles (< 10 µm), ~ 5 intermediate particles (~ 50 to 100 µm) and ~ 1 is large particles (> 200 µm). The total volume of each size fraction is

Table 2 Volume percentage of small (<10 μm), intermediate (~50 to 100 μm) and large (>200 μm) particles for both pre- and post-test proppants

	Pre-test (%)	Post-test (%)
Small (<10 μm)	0.03	0.50
Intermediate (~50 to 100 μm)	2.44	19.90
Large (>200 μm)	97.53	79.50

calculated by Eq. (1). The calculation indicates that the total volume of large particles is ~10 times that of that of intermediate particles, and ~100 times that of the small particles. Comparing the pre- and post-test PSDs in terms of cumulative percentage by number, there is an increase in that of the small particles from 25 out of 100 to 50 and a large decrease in that of the large particles from 10 out of 100 to 1.

Assuming the total volume is only comprised of that of the three defined families, the percentage of each in total volume is shown in Table 2.

In contrast to the great change in number percentages, the volume percentage of each size fraction show less variations that the volume of large particle still takes up the majority of the total volume (~80%). This suggests that even though large particles break and produce a great number of small particles as a result of extensive crushing, the volume percentage of each size fraction is relatively invariant.

3.5 Long-Term Behavior

Long-term conductivity tests used proppants at two contrasting loading concentrations of 1.22 kg/m^2 and 2.44 kg/m^2 . Testing conditions and procedures are identical to those for the previous conductivity measurements except for the holding time for each effective stress step—extended from 25 min to 24 h. The long-term equivalent permeability

Table 3 Surface roughness parameters of pre- and post-test fracture surface after both short-term and long-term experiments

Sample #	$S_a(\mu\text{m})$	$S_q(\mu\text{m})$	$S_z(\mu\text{m})$
Ground pre-test	0.43	0.56	6.25
2.44 kg/m^2 post-test (short-term)	6.93	8.71	57.59
2.44 kg/m^2 post-test (long-term)	7.85	9.82	64.26

(Fig. 15a) exhibits a comparable trend and magnitudes to that for the short-term measurements (Fig. 15b).

Table 3 compares the surface roughness parameters for the ground pre-test surface relative to the post-test fracture surfaces for both short-term and long-term experiments, respectively. The proppant loading concentrations are for the higher load of 2.44 kg/m^2 for both experiments. This shows a 12% increase in embedment depth (S_q) as a result of long-term exposure, presumably due to rock creep. However, the embedment depth remains rather small compared to the entire thickness of the proppant pack, inferring a negligible influence on conductivity evolution.

4 Discussion

The experimental observations demonstrate that effective stress, proppant loading concentration, proppant embedment, proppant crushing, compaction and rearrangement all significantly and systematically influence conductivity/permeability evolution of propped fractures. However, the relative contribution of these factors varies, dependent on specific circumstances.

The reduction in conductivity by 95% observed in our experiments, over the stress range 6.9 to 55.2 MPa is congruent with the percentage reduction observed in other experiments and over a similar stress range (Barree et al. 2003; Palisch et al. 2007)—although the absolute magnitudes

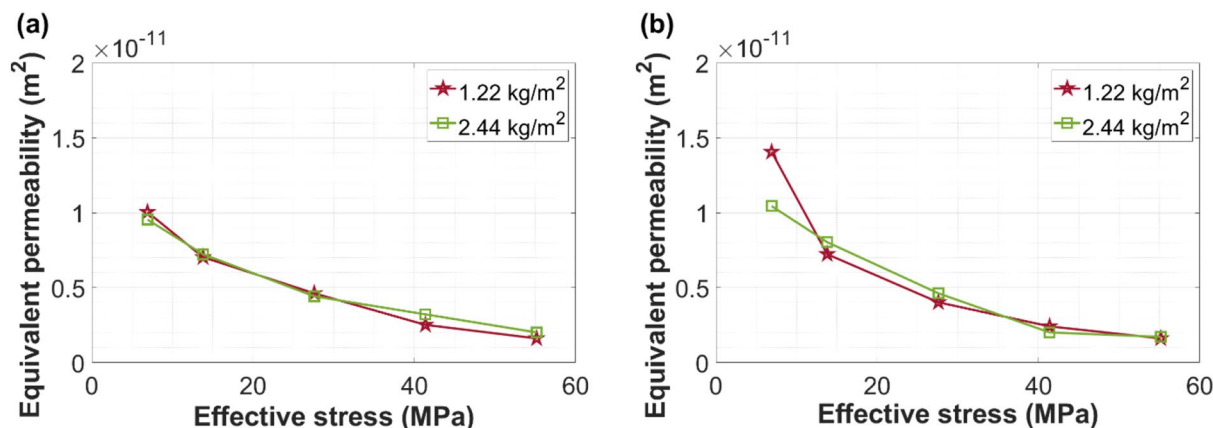


Fig. 15 Evolution of equivalent permeability during both: **a** long-term and **b** short-term experiments

of permeability change are different due to the variability between the mechanical properties of fracture and proppant materials.

Under low effective stress (6.9 MPa), the low proppant loaded fracture conductivity (Fig. 10) is significantly reduced by proppant embedment by up to 60%, while the higher proppant loaded fracture is insignificantly affected. However, one counter-intuitive observation is that a lower proppant loading concentration results in a much higher permeability (Fig. 6(a))—representing the transmission capacity of the proppant pack as a porous medium. This is in contrast to prior arguments that arrangements of proppants in multiple layers allow more contact points to resist stress and favors minimal loss of proppant pack conductivity (Elsarawy and Nasr-El-Din, 2018). We posit that the increased number of contact points may also result in denser packing and a reduction in pore throat diameter—as a result of the increase in displacement degree of freedom as the pack thickens—allowing particle rearrangement and denser packing. Considering that proppant crushing and embedment effects are both trivial for the high concentration fracture, we conclude that greater interior compaction and grain rearrangement are the dominant mechanisms contributing to the observed reduction in permeability, resulting from a loss in porosity.

The Kozeny–Carman equation defines fluid flow through a packed bed (Foust et al. 2008; Kruczek 2014) and relates pressure drop to pack porosity, as:

$$\frac{\Delta p}{L} = \frac{180\mu}{\phi_s^2 D_p^2} \frac{(1 - \epsilon)^2}{\epsilon^3} v_s, \tag{7}$$

where Δp (Pa) is the differential pressure, L (m) is the length of the packed bed along the fluid flow, μ (Pas) is the viscosity of fluid, ϕ_s is the sphericity of the particles, D_p is the diameter of particles, v_s (m/s) is the superficial fluid flow velocity (real fluid flow velocity for single-phase flow), and ϵ is the pack porosity. Combining the Kozeny–Carman Eq. (7) with Darcy’s law of Eq. (2) relates hydraulic conductivity C to the porosity of the proppant pack ϵ , sphericity of the particles ϕ_s and the particle diameter D_p , as:

$$C = \frac{\phi_s^2 D_p^2}{180} \frac{\epsilon^3}{(1 - \epsilon)^2} h, \tag{8}$$

where h (m) is the fracture aperture.

The PSD changes significantly as a result of proppant loading concentration and stress (Fig. 10a), enabling the Kozeny–Carman relation to represent the change in conductivity as a result of particle rupture. We select the 80th percentile particle size and circularity for each proppant concentration as representative particle diameter D_p and sphericity ϕ_s . Sphericity is related to the 2D proxy of circularity (Berrezueta et al. 2019), enabling substitution of circularity

Table 4 Proppant pack porosity at 55.2 MPa

Proppant loading concentration	0.49 kg/m ²	1.22 kg/m ²	2.44 kg/m ²	4.88 kg/m ²
Proppant porosity at 55.2 MPa (%)	53.41	56.52	52.89	49.85

for sphericity in Eq. (8), corresponding to the various proppant loading concentrations. This enables proppant pack porosity of each proppant loading concentration scenario at 55.2 MPa to be calculated (Table 4) from Eq. (8) where conductivity of the sample is as measured (Fig. 5(a)).

The porosity distribution of Table 4 indicates that under high effective stress (55.2 MPa) the overall porosity decreases with increasing proppant loading concentration, except for the lowest proppant loading concentration scenario (0.49kg/m²) that exhibits a slightly lower pack porosity. Porosities are not independently measured at test-end and any estimates suffer the intrinsic limitations of the Kozeny–Carman relation (Costa 2006; Chen et al. 2018). Previous observations of the applicability of the Kozeny–Carman relation indicate a functional reliability for reservoir rocks with high porosity (~0.45), no or little cement and relatively homogeneous particle size (Han et al. 2019)—factors replicated for this uniformly fabricated and homogeneous proppant pack.

For high proppant loading concentration, embedment and proppant crushing are both significantly attenuated (Figs. 10 & 11). The decrease in proppant pack porosity with increasing proppant loading concentration indicates a progressive impact of interior compaction and rearrangement. This is likely attributed to the additional displacement degree of freedom accorded as the proppant pack gets thicker—enabling compaction to generate a more efficient packing and reduced porosity. Thus, a threshold concentration loading will exist, above which, proppant permeability will remain effectively constant. This conjecture is supported by observations of permeability evolution for the rigid steel platens as shown in Fig. 6b—where ultimate permeabilities are comparable for all proppant loading concentration scenarios.

The lowest proppant loading concentration scenario (0.49 kg/m² for Fig. 9) shows a significant (76%) reduction in fracture conductivity due to proppant embedment. The influence of embedment is also supported by post-test analysis where the RMS amplitude S_q (Fig. 9b) shows an average proppant embedment depth of 10.54 μ m on each side of the fracture walls, and the PSD (Fig. 11a) indicates that 80% of the particles, post-test, are less than 13.73 μ m in diameter. If we consider the proppant loading concentration in terms of multiple layers, the average aperture change

for this double layer scenario is more than 75%. Therefore, we conclude that, for fractures supported by low concentrations of proppant, embedment severely impairs conductivity by significantly decreasing mean fracture aperture. This is also in agreement with the abnormally low porosity recovered from the conductivity (Table 4), that even though the particle compaction and rearrangement is minor compared with the higher proppant loading concentration scenarios, the effect of embedment is too extensive and results in an even lower porosity.

Furthermore, a significant distinction of this study is the selection of proppant. Distinct from the proppants commonly used in laboratory experiments, where PSDs are narrow and particle sizes largely uniform (e.g., for 30/50 and 40/70 mesh sands) (Briggs et al. 2014; Zhang et al. 2015; Zheng and Tannant 2016), the PSDs of the proppant used in this study is much more broadly graded (Fig. 2). This broader PSD results in intrinsic tendency for denser packing and reduced permeability.

There is no apparent change in conductivity over the long-term holds (of stress) used in this study. This is distinct from other complementary studies that suggest much larger decreases in conductivity during long-term experiments (24 h to 1000 days). Considering the role of mechanical stresses and the chemistry of pore fluids under elevated temperature as agents of proppant diagenesis, propped hydraulic fractures exhibit permeability decline of only a few percent over periods of tens of days but tens of percent over longer periods (say 1000 days) under in situ stress (Lee et al. 2010).

Possible reasons for this minimal observed change in permeability in this study include as a result of: (i) only intermittent fluid flow through the fracture during a portion of the hold-time (when the stress is retained constant) when the syringe pump requires to be refilled; (ii) the 24-h hold-time being too short for significant mineral dissolution and redeposition, even where pressure solution (driven by stress) is activated (Yasuhara et al. 2003; Lee et al. 2010), (iii) temperatures (20 °C) (Lee et al. 2010) being too low to activate significant pressure solution effects, and (iv) smaller sized proppant is more likely prone to crushing with the potential for blocking of pore throats. The reduction in permeability increases from 30% to an unusually high magnitude of 99% as proppant size decreases from 20/40 to 60/100 (Mittal et al. 2018)—this is also consistent with more rapid activation of pressure solution as grain size decreases.

5 Conclusions

This study investigates the evolution of propped fracture conductivity/permeability as a function of proppant loading concentration under varying effective stresses as an analog to reservoir drawdown. In particular, the relative impacts and

interplay between proppant crushing, embedment, compaction and rearrangement and their impacts on fluid transport are studied. Based on the studies, the following conclusions are made:

- (1) Fracture conductivity decreases by up to 95% when the effective pressure increases by 48.3 MPa. The sensitivity of conductivity to stress gradually reduces with increasing effective stress.
- (2) Reduced proppant loading concentration results in greater proppant embedment, increased proppant crushing and greater circularity.
- (3) The mechanisms for permeability reduction between different proppant loading concentrations (thicknesses) are different. Low proppant loading concentration supporting a shale fracture returns high permeability at low effective stresses, but diminishes rapidly with increased stress where the dominant impairment mechanism is proppant embedment in the fracture wall. A higher loading concentration of proppant is less stress sensitive and maintains a higher permeability under high effective stress, for which the major factor reducing permeability is proppant compaction.
- (4) Extending the holding time for the effective stress (from 25 min to 24 h) has little impact on the trend and magnitude of evolution in fracture conductivity at room temperature from the tests conducted in this work. Possible reasons include the intermittent fluid flow through fracture, insufficient holding time and low experimental temperature (20 °C), potentially attenuating any porosity reduction induced by pressure solution or other thermally activated and fluid mediated mechanisms.

The above provide insights into the selection and application of proppants for hydraulic fracturing. Where proppants can only be injected into the fracture at low loading concentrations, the most effective approach to maintain fracture permeability is to reduce proppant embedment. Possible techniques include injecting appropriate shale inhibitors to reduce shale swelling (Koteeswaran et al. 2018) and using larger sized higher Young's modulus proppants (Ming et al. 2018). Where high proppant loading concentrations are attained, the major impairment mechanism is proppant compaction and rearrangement, which could be possibly attenuated by using monodisperse proppants with a narrow PSD or preventing the generation of fines by using proppant with a higher resistance to crushing (Zhang et al. 2015). Furthermore, it is useful to define the threshold proppant loading concentration, above which, permeability is insensitive to increasing concentration of proppant. Another consideration is to select proppant loading concentration based on the in-situ stress, as the relative performance of proppants vary during different stages of reservoir pressure drawdown.

Acknowledgements This work was supported by Chevron ETC. This support is gratefully acknowledged.

Declarations

Conflict of interest The authors declare that they have no conflicts of interest.

References

- Alramahi B, Sundberg MI (2012) Proppant embedment and conductivity of hydraulic fractures in shales. In: 46th US Rock Mechanics/ Geomechanics Symposium. American Rock Mechanics Association, 2012.
- Arthur JD, Bohm B, Layne M (2009) Hydraulic fracturing considerations for natural gas wells of the Marcellus Shale.
- Barree RD et al (2003) Realistic assessment of proppant pack conductivity for material selection. In: SPE Annual Technical Conference and Exhibition. OnePetro, 2003
- Beckwith R (2011) Proppants: where in the world. *J Petrol Technol* 63(04):36–41
- Berrezueta E et al (2019) Representativity of 2D shape parameters for mineral particles in quantitative petrography. *Minerals* 9(12):768
- Briggs K et al (2014) The relationship between rock properties and fracture conductivity in the Fayetteville shale. In: SPE Annual Technical Conference and Exhibition. Society of Petroleum Engineers, 2014
- Chen X et al (2018) Pore-scale determination of gas relative permeability in hydrate-bearing sediments using X-ray computed microtomography and lattice Boltzmann method. *Water Resour Res* 54(1):600–608
- Cikes M (1996) Long-term hydraulic fracture conductivities under extreme conditions. In: European Petroleum Conference. Society of Petroleum Engineers, 1996
- Costa A (2006) Permeability-porosity relationship: A reexamination of the Kozeny–Carman equation based on a fractal pore-space geometry assumption. *Geophys Res Lett* 33(2). <https://doi.org/10.1029/2005GL025134>
- Elsarawy AM, Nasr-El-Din HA (2018) Proppant performance in marcellus shale fractures under experimental in-situ stress conditions. In: SPE/IADC Middle East Drilling Technology Conference and Exhibition. Society of Petroleum Engineers, 2018.
- Foust AS et al (2008) Principles of unit operations. Wiley
- Han D et al (2019) Analysis of the Kozeny–Carman model based on pore networks. *J Geophys Eng* 16(6):1191–1199
- Koteeswaran S et al (2018) Characterization of shale–fluid interaction through a series of immersion tests and rheological studies. *J Pet Explor Prod Technol* 8(4):1273–1286
- Kruczek B (2014) Carman–kozeny equation. *Encyclopedia of membranes*, pp 1–3.
- Kurz BA, Schmidt DD, Cortese PE (2013) Investigation of improved conductivity and proppant applications in the Bakken formation. In: SPE Hydraulic Fracturing Technology Conference. Society of Petroleum Engineers, 2013
- Lee DS et al (2010) Experiment and modeling to evaluate the effects of proppant-pack diagenesis on fracture treatments. *J Pet Sci Eng* 74(1–2):67–76
- Liang F et al (2016) A comprehensive review on proppant technologies. *Petroleum* 2(1):26–39
- Mayerhofer MJ, et al (2006) Integration of microseismic-fracture-mapping results with numerical fracture network production modeling in the Barnett Shale. In: SPE annual technical conference and exhibition. OnePetro, 2006
- Meyers RA (1982) The macromolecular structure of coal: coal structure. Academic Press Inc., New York, p 250
- Ming CHEN et al (2018) Calculation method of proppant embedment depth in hydraulic fracturing. *Pet Explor Dev* 45(1):159–166
- Mittal A, Rai CS, Sondergeld CH (2018) Proppant-conductivity testing under simulated reservoir conditions: impact of crushing, embedment, and diagenesis on long-term production in shales. *SPE J* 23(04):1–304
- Palisch TT, et al (2007) Determining realistic fracture conductivity and understanding its impact on well performance-theory and field examples. In: SPE Hydraulic Fracturing Technology Conference. Society of Petroleum Engineers, 2007
- Pope C et al (2009) Haynesville shale—one operator's approach to well completions in this evolving play. In: SPE Annual Technical Conference and Exhibition. Society of Petroleum Engineers, 2009.
- Terracina JM, et al (2010) Proppant selection and its effect on the results of fracturing treatments performed in shale formations. In: SPE Annual Technical Conference and Exhibition. Society of Petroleum Engineers, 2010
- Vengosh A et al (2014) A critical review of the risks to water resources from unconventional shale gas development and hydraulic fracturing in the United States. *Environ Sci Technol* 48(15):8334–8348
- Wang J, Elsworth D (2018) Role of proppant distribution on the evolution of hydraulic fracture conductivity. *J Pet Sci Eng* 166:249–262. <https://doi.org/10.1016/j.petrol.2018.03.040>
- Weaver JD et al (2007) Fracture-related diagenesis may impact conductivity. *SPE J* 12(03):272–281
- Wen Q et al (2007) The effect of proppant embedment upon the long-term conductivity of fractures. *J Pet Sci Eng* 55(3–4):221–227
- Yasuhara H, Elsworth D, Polak A (2003) A mechanistic model for compaction of granular aggregates moderated by pressure solution. *J Geophys Res Solid Earth* 108(B11)
- Zhang J et al (2013) Laboratory measurement of hydraulic fracture conductivities in the Barnett shale. In: IPTC 2013: International Petroleum Technology Conference. European Association of Geoscientists & Engineers, 2013
- Zhang F et al (2017) Discrete-element-method/computational-fluid-dynamics coupling simulation of proppant embedment and fracture conductivity after hydraulic fracturing. *Spe J* 22(02):632–644
- Zhang J, Zhu D, Hill AD (2015 February) Water-induced fracture conductivity damage in shale formations. In SPE Hydraulic Fracturing Technology Conference. OnePetro.
- Zheng W, Tannant D (2016) Frac sand crushing characteristics and morphology changes under high compressive stress and implications for sand pack permeability. *Can Geotech J* 53(9):1412–1423

Publisher's Note Springer Nature remains neutral with regard to jurisdictional claims in published maps and institutional affiliations.